

Calculation of the electron-impact-ionization cross section of helium including electron correlations

Cheng Pan and Hugh P. Kelly

Department of Physics, University of Virginia, Charlottesville, Virginia 22901

(Received 25 May 1989)

The total cross section and the single-differential cross section in energy for the ionization of the ground-state helium atom by electron impact have been calculated in distorted-wave approximations. The optical potential, or self-energy of the single-particle Green's function, was used to investigate effects of electron correlations in the initial state. Our results are compared with the results of experiments and other calculations.

I. INTRODUCTION

There has been increasing theoretical interest in ionization of atoms and atomic ions by electron impact because accurate electron-impact-ionization cross sections are needed for plasma research^{1,2} and also because the impact-ionization processes present interesting problems for studies of the effects of interactions in many-electron systems.³⁻⁷ Efforts have been made in recent calculations to include effects of electron correlations. For example, Jakubowicz and Moores² used close-coupling wave functions to include interactions between ionization channels and effects of autoionization in their calculation of total cross sections for Li-like and Be-like ions. Bartschat and Burke⁶ used the *R*-matrix method to study correlation effects, including effects of autoionization as well as ionization with simultaneous excitation in their calculation of the impact-ionization cross section of helium. In several calculations of the triple-differential cross sections of hydrogen and helium for small momentum transfer, higher-order effects were treated by different methods.⁵

In this paper we present a study of the total cross section σ and single-differential (in energy) cross section $d\sigma/d\varepsilon$ for helium for incident electron energies between the ionization threshold at 24.6 and 800 eV. We used the optical potential method⁸ to study effects of electron correlations. Distorted-wave states were used as basis states to evaluate the perturbation expansion of the optical potential. In addition to a distorted-wave exchange approximation, we investigated electron correlation effects in the initial state, which are effects of the virtual excitations involving both of the 1s electrons in helium. Our results of the total and single-differential (in energy) cross sections agree reasonably with results of other distorted-wave approximations^{3,7} which show improved agreement with experiments⁹⁻¹¹ in comparison with the results of first Born approximation.¹²⁻¹⁷

The electron-impact-ionization cross section of helium in first Born approximation has been studied extensively,¹²⁻¹⁷ and the calculations have been reviewed by Bell and Kingston^{12,13} and by Economides and McDowell.¹⁴

Bransden *et al.*¹³ previously used distorted-wave ap-

proximations to calculate the total and differential cross sections of helium for incident energies between 100 and 400 eV. They used adiabatic approximations and polarization potentials in evaluating the outgoing waves. They evaluated the incident waves with a second-order, nonlocal, and complex potential derived using a closure approximation, and according to their conclusion the closure approximation became inaccurate at energies below 150 eV. A very recent calculation using a distorted-wave approximation was carried out by Campeanu *et al.*,⁷ who included polarization potentials in evaluating the continuum wave functions and calculated the total cross section of helium for incident energies between 40 and 400 eV. We became aware of their work after we completed the calculations presented in this paper.

For incident energies of several electron volts in excess of the threshold energy, wave functions based on the assumption of complete screening of the residual ion by the slower outgoing electron do not provide reasonable results for the total cross section of helium.¹³ We also evaluated wave functions for each outgoing electron in a potential which approximates the interaction experienced by the electron assuming partial screening of the residual ion by the other outgoing electron. The total cross section we obtained using these wave functions agrees reasonably well with experimental results near threshold.

We review the theory in Sec. II. In Sec. III our results are compared with the results of experiments and other calculations. Our conclusions are given in Sec. IV.

II. THEORY

The general theory of electron-impact ionization of atoms and atomic ions has been reviewed by Rudge.¹⁸ The expressions of total and differential cross sections are derived using the transition amplitude constructed by considering the asymptotic wave functions which satisfy the boundary conditions specified by the impact-ionization process. We review the relations of the total cross section σ and the single-differential (in energy ε) cross section $d\sigma/d\varepsilon$ with the optical potential for the scattering electron. Atomic units are used throughout this paper.

As discussed by many authors,^{8,19} the optical potential

is the proper self-energy of the single-particle Green's function, which represents the probability amplitude for the propagation of a particle (or a hole) in a many-body system. This proper self-energy contains effects of interactions between the particle and the rest of the system, and it can be calculated by a many-body perturbation expansion.^{8,19,20} The optical potential method has been applied to problems of electron scattering by atoms.^{8,21,22}

In the nonrelativistic case, the optical potential V_{op} in the Schrödinger equation for the exact scattering wave function,

$$(-\frac{1}{2}\nabla^2 + V_{\text{op}})\psi_k = \frac{1}{2}k^2\psi_k, \quad (1)$$

may be written as

$$V_{\text{op}} = V_{\text{op}}^{(0)} + V'_{\text{op}}, \quad (2)$$

where $V_{\text{op}}^{(0)}$ includes the interaction with the nucleus and an average interaction with all other electrons and V'_{op} is treated as a perturbation due to electron correlations.

The basis states used in perturbation calculations are solutions of the single-particle Schrödinger equation

$$(-\frac{1}{2}\nabla^2 + V_{\text{op}}^{(0)})|k\rangle = \varepsilon_k|k\rangle, \quad (3)$$

where the potential $V_{\text{op}}^{(0)}$ may contain a projection operator when needed to ensure the orthogonality of the basis wave functions.²³

The matrix element $\langle k|V'_{\text{op}}|k\rangle$ may be expanded by many-body diagrams,^{8,19-22} and low-order diagrams are shown in Fig. 1. The horizontal dashed lines in these diagrams represent the Coulomb interaction $v=1/r_{ij}$ between electrons i and j . Lines with arrows drawn upward

denote continuum and bound excitations (particles), and lines with arrows drawn downward represent vacancies (holes) in the initial state. The external particle lines on the bottom and top of each diagram are lines of the same state $|k\rangle$, which represents a partial-wave component of the scattering electron. The order of a diagram refers to the number of Coulomb-interaction lines in it. The first-order diagrams of Figs. 1(a)–1(c) sum to zero when the Hartree-Fock potential plus the nuclear potential is used as $V_{\text{op}}^{(0)}$ in Eq. (3). Figures 1(d)–1(g) are the second-order diagrams contributing to $\langle k|V'_{\text{op}}|k\rangle$. Figures 1(d) and 1(e) contain imaginary parts, which are related to inelastic events including impact ionization, provided that the energy is high enough. The diagrams in Fig. 1 which contain only real results will not be discussed further. For simplicity we consider only the scattering of electrons by closed-shell atoms.

The contribution of Fig. 1(d) is

$$V_{\text{op}}^{(2)} = \sum_{p,k_1,k_2} \frac{\langle kp|v|k_1k_2\rangle\langle k_1k_2|v|kp\rangle}{\varepsilon_k + \varepsilon_p - \varepsilon_{k_1} - \varepsilon_{k_2}}, \quad (4)$$

where p denotes a hole, and k_1 and k_2 denote two particle states. Note that ε_k is the energy of the scattering electron. The summation over k_1 and k_2 is understood as including a summation over the bound excited states and an integration over the continuum. Figure 1(e) is the exchange diagram of Fig. 1(d), and its contribution is given by replacing $\langle kp|v|k_1k_2\rangle$ in Eq. (4) by $-\langle pk|v|k_1k_2\rangle$.

We can also combine contributions of Figs. 1(d) and 1(e) by writing

$$V_{\text{op}}^{(2)} = \sum_{\Phi_p^{k_1k_2}} \frac{\left| \left\langle \Phi_p^{k_1k_2} \left| \sum_{i<j=1}^N \frac{1}{r_{ij}} \right| \Phi^k \right\rangle \right|^2}{E(k) - E(p^{-1}k_1k_2)}, \quad (5)$$

where Φ^k is the wave function of the initial state consisting of the scattering electron k and the ground-state atom, and $\Phi_p^{k_1k_2}$ is the wave function of an excited state of the system including electrons in excited states k_1 and k_2 and the ionic core with electron p missing from the atom. Both states Φ^k and $\Phi_p^{k_1k_2}$ are LS -coupled wave functions which are linear combinations of determinants constructed with the basis orbitals, and $E(k)$ and $E(p^{-1}k_1k_2)$ denote the lowest-order energies of these two states, respectively.

The energy denominators in Eqs. (4) and (5) vanish when the energy of state $\Phi_p^{k_1k_2}$ is degenerate with the energy of state Φ^k . In such a case Eqs. (4) and (5) include processes other than elastic scattering. If both k_1 and k_2 are continuum states, then the process is impact ionization. If one of k_1 and k_2 is a bound state and the other is a continuum state, the process is inelastic scattering with impact excitation, and if both k_1 and k_2 are bound excitations, there is an autoionizing resonance. The singularity related to impact ionization or impact excitation is treated by introducing an infinitesimal imaginary term $i\eta$ in the denominator D in Eq. (4) or Eq. (5) and writing

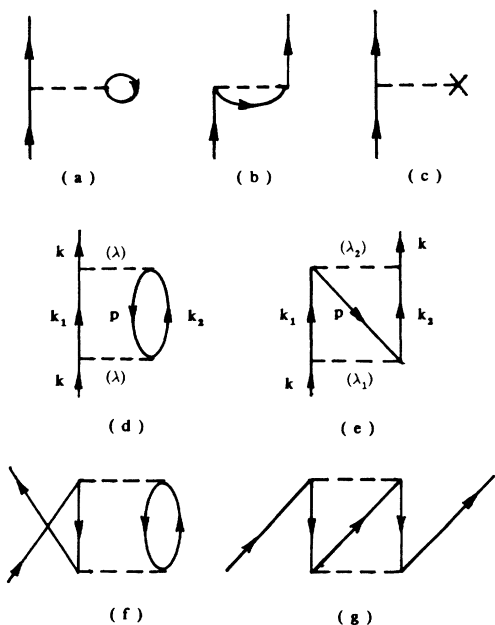


FIG. 1. First- and second-order diagrams for $\langle k|V'_{\text{op}}|k\rangle$. First-order diagrams (a), (b), and (c) add to zero when $V_{\text{op}}^{(0)}$ is chosen to be the Hartree-Fock potential plus the nuclear potential. Diagrams (d) and (e) contribute imaginary part to the matrix element of V'_{op} .

$$\lim_{\eta \rightarrow 0^+} \frac{1}{D + i\eta} = P \frac{1}{D} - i\pi\delta(D), \quad (6)$$

where P represents principal-value integration. The result of Eq. (4) or Eq. (5) contains an imaginary part after applying Eq. (6).

The imaginary part V'_1 of the optical potential is due to the effects of inelastic processes, and we may calculate the cross section of the inelastic events using V'_1 . When V'_1 is not zero, the continuity equation obtained from the time-dependent Schrödinger equation is²⁴

$$\frac{d\rho}{dt} + \nabla \cdot \mathbf{j} = 2\psi_k^* V'_1 \psi_k, \quad (7)$$

where ρ and \mathbf{j} are the probability density $\psi^*\psi$ and the probability current density $\text{Re}(-i\psi^*\nabla\psi)$ for electrons with wave number k , respectively. Integrating Eq. (7) over a large sphere with radius R and letting $R \rightarrow \infty$ afterwards, we have the rate of change of the total probability for electrons with wave number k ,

$$I = 2\langle \psi_k | V'_1 | \psi_k \rangle, \quad (8)$$

and $-I$ can be interpreted as the rate of inelastic events. The rate $-I$ can be evaluated by perturbation calculations.

The scattering wave constructed from a partial-wave expansion using the basis states from Eq. (3) is

$$\phi_k = \frac{4\pi}{k} \sum_{l=0}^{\infty} \sum_{m=-l}^l i^l e^{i(\sigma_l + \delta_l)} Y_{lm}^*(\hat{\mathbf{k}}) |k\rangle, \quad (9)$$

where σ_l and δ_l are the Coulomb and non-Coulomb phase shifts, respectively. The state $|k\rangle$ is given by $R_{kl}(r)Y_{lm}(\hat{\mathbf{r}})\chi(m_s)$, where χ is the spin wave function. The radial wave function R_{kl} is normalized according to

$$rR_l(r) \rightarrow \sin \left[kr + \frac{q}{k} \ln(2kr) - \frac{l\pi}{2} + \sigma_l + \delta_l \right], \quad (10)$$

as $r \rightarrow \infty$. In Eq. (10), q is the asymptotic charge of the potential $V_{\text{op}}^{(0)}$, and for the potential field of a neutral atom both q and σ_l are zero. Using ϕ_k to calculate the rate of inelastic events, the cross section for inelastic processes is

$$\sigma = -\frac{2}{k} \langle \phi_k | V'_1 | \phi_k \rangle. \quad (11)$$

Substituting Eq. (9) into Eq. (11) and integrating over angular coordinates, we have

$$\sigma = \frac{32}{k^3} \sum_{l,p,\alpha} (2l+1) \int_0^{\varepsilon_k + \varepsilon_p} \frac{1}{k_1 k_2} \left| \left\langle \Phi_p^{k_1 k_2} \left| \sum_{i < k=l}^N \frac{1}{r_{ij}} \right| \Phi^k \right\rangle \right|^2 d \left[\frac{k_2^2}{2} \right], \quad (13)$$

where ε_p is the negative of the lowest-order ionization energy associated with electron p , and k_1 is related to k_2 by

$$\frac{k_1^2}{2} + \frac{k_2^2}{2} = \varepsilon_k + \varepsilon_p. \quad (14)$$

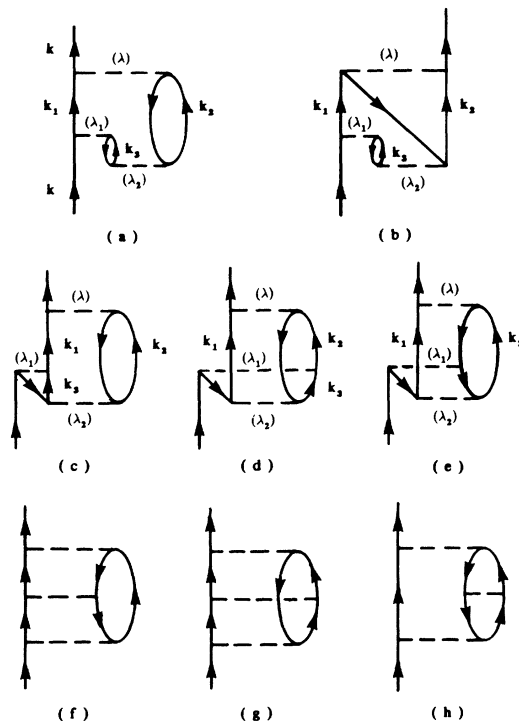


FIG. 2. Some of the third-order diagrams for $\langle k | V'_{\text{op}} | k \rangle$. Diagrams (a)–(e) include correlation effects in the initial state of the ionization process, and diagrams (f), (g), and (h) include correlation effects in the final states. Time runs from bottom to top in the diagrams. The diagrams of the other time orderings of diagrams (a)–(e) are not shown but understood to be included.

$$\sigma = -\frac{8\pi}{k^3} \sum_{l=0}^{\infty} (2l+1) \langle k | V'_1 | k \rangle. \quad (12)$$

The matrix element $\langle k | V'_1 | k \rangle$ is the imaginary part of $\langle k | V'_{\text{op}} | k \rangle$, which is expanded by diagrams including those in Figs. 1 and 2.

We will consider only the case when both k_1 and k_2 in Figs. 1 and 2 are continuum orbitals since electron-impact ionization is our concern in this paper. The intermediate states $\Phi_p^{k_1 k_2}$ in the diagrams in Figs. 1 and 2 are the final states of the impact-ionization process. Substituting into Eq. (12) the imaginary part of Eq. (5) obtained by completing the integration with respect to k_1 using Eq. (6), the ionization cross section including the contributions of Figs. 1(d) and 1(e) is

In Eq. (13), α represents implicitly the angular momentum couplings of the final state and the l values of electrons k_1 and k_2 . Also, Eq. (13) depends upon the normalizations of radial wave functions of electrons k_1 and k_2 according to Eq. (10).

An often used approximation in calculations of electron-impact-ionization cross sections is to assume complete screening of the residual ion by the slower outgoing electron. In this approximation the orbitals of the slower and faster outgoing electrons are evaluated in two

different potentials which represent a bare residual ion and a completely screened residual ion, respectively. For these orbitals the cross section including contributions of Figs. 1(d) and 1(e) may be written as

$$\sigma = \frac{32}{k^2} \sum_l \sum_{p, l_1, l_2} (2l+1) \int_0^{(\epsilon_k + \epsilon_p)/2} \frac{1}{k_> k_<} (|\langle k_> k_< | v | k p \rangle|^2 + |\langle k_< k_> | v | k p \rangle|^2 - 2 \langle p k | v | k_> k_< \rangle \langle k_> k_< | v | k p \rangle) d \left[\frac{k_<^2}{2} \right], \quad (15)$$

where $k_<$ and $k_>$ are the smaller and the larger of k_1 and k_2 related by Eq. (14), respectively. The first two terms in the parentheses in Eq. (15) correspond to Fig. 1(d), and the last term corresponds to Fig. 1(e). The single-differential (in energy ϵ) cross section $d\sigma/d\epsilon$ for $\epsilon < (\epsilon_k + \epsilon_p)/2$ is obtained by dropping the integration sign in Eq. (15) and letting $\epsilon = k_<^2/2$. The results of $d\sigma/d\epsilon$ for ϵ values between $(\epsilon_k + \epsilon_p)/2$ and $\epsilon_k + \epsilon_p$ are obtained from the results for $\epsilon < (\epsilon_k + \epsilon_p)/2$ by a mirror reflection about $(\epsilon_k + \epsilon_p)/2$. The contributions of the third-order diagrams in Fig. 2 can be discussed similarly.

The diagrams of Figs. 2(a) through 2(e) contain intermediate states in which both of the $1s$ electrons in helium are excited. In each of these diagrams the external particle line entering the diagram does not terminate at the lowest interaction line, and these diagrams describe electron correlation effects in the initial state. In this study we calculated these diagrams and the other time ordering of these diagrams. The diagrams of Figs. 2(f), 2(g), and 2(h) contain interactions between final states of impact-ionization processes. Strong cancellations occur among these diagrams when the two excited orbitals are evaluated assuming that the residual ion is completely screened by one of the excited electrons and the other electron experiences the field of an atom.²⁵ Each of the three diagrams has a singularity when the energies of the intermediate states are the same as the initial state. With the numerical wave functions used in this study, it was difficult to perform the summations for these diagrams. We did not compute diagrams such as Figs. 2(f), 2(g), and 2(h) but chose potentials which cause relatively strong cancellations among these diagrams.

When describing the final-state wave function of the ionization process of atoms due to electron impact by use of single-electron wave functions, a relation¹⁸ which ensures the convergence of the phase factor in the usual integral expression of the scattering amplitude is

$$\frac{z_1}{k_1} + \frac{z_2}{k_2} = \frac{1}{k_1} + \frac{1}{k_2} - \frac{1}{|\mathbf{k}_1 - \mathbf{k}_2|}, \quad (16)$$

where z_i is the asymptotic charge experienced by outgoing electron i , and \mathbf{k}_i is the momentum of electron i ($i=1,2$). The asymptotic charges depend on the angle between the two momenta \mathbf{k}_1 and \mathbf{k}_2 . Thus far in calculations of ionization cross sections, wave functions have been evaluated in potentials which do not satisfy Eq. (16)

rigorously, and different approximations have been made.^{1-3,18}

In the Born approximation,¹⁸ plane-wave states are used for the incident electron and the faster outgoing electron, and the wave function of the slower outgoing electron is evaluated in a potential with unit asymptotic charge. The fast electron is assumed to interact with a residual ion completely screened by the slower electron. In the modified Born approximation,^{12,18} the exchange contributions to the total cross section are approximately included by integrating over the kinetic energy of the ejected electron from zero to only half the maximum possible value, that is, by truncating the integration interval for the direct contributions at half the full range. In the Born-exchange approximation,^{18,26} both exchange and direct contributions are evaluated. In the distorted-wave approximation, wave functions of electrons may be evaluated in various potentials which model the average interactions experienced by the electrons.¹⁻³

In low-order calculations wave functions based on the assumption of complete screening of the residual ion by the slower outgoing electron are good for high incident energies. In the relation given by Eq. (16), when $k_1 > k_2$ we have $z_1 = 0$ and $z_2 = 1$ in Born approximation, and the equation is approximately satisfied if $k_1 \gg k_2$, which is the case experimentally observed to dominate the probability at high incident energies.

III. CALCULATIONS AND RESULTS

We calculated the total cross section σ and the single-differential cross section $d\sigma/d\epsilon$ for impact ionization of helium by electrons with energies ranging from the threshold up to 800 eV. We used the negative of the Hartree-Fock energy $-\epsilon_{1s}$ as the ionization energy, and $-\epsilon_{1s}$ is 24.98 eV, which is about 0.4 eV larger than the 24.6-eV experimental ionization energy.⁹ We did not calculate the impact-double-ionization cross section which is experimentally known to be no more than 1% of the total cross section for helium,^{27,28} and we also did not include impact ionization with excitation which is also weak.⁶

For the incident electron, the $1s$ electrons in both the initial and final states, and the faster one of the two outgoing electrons, the wave functions were evaluated using Eq. (3) with the potential $V_{op}^{(0)}$ given by

$$V_1 = 2J_{1s}^0 - \frac{1}{2l+1} K_{1s}^l - \frac{2}{r}, \quad (17)$$

where J_{1s}^0 and K_{1s}^l are the usual direct and exchange operators. The potential we used for the slower outgoing electron was

$$V_2 = V_1 + (1 - |1s\rangle\langle 1s|) \left[J_{1s}^0 + \frac{1}{2l+1} K_{1s}^l - \frac{2}{r} - V_1 \right] \times (1 - |1s\rangle\langle 1s|), \quad (18)$$

where the projection operator²³ ensures that the ks orbitals evaluated from this potential are orthogonal to the $1s$ orbital based on Eq. (17). Equation (17) gives the potential experienced by an electron which interacts with the neutral He atom, and Eq. (18) gives the potential experienced by an electron kl which couples with a He^+ ion to $1skl(^1L)$ states ($L=l$). Thus for each of the outgoing electrons we have a complete set of orbitals reflecting the complete screening of the residual ion by the slower outgoing electron.

For each incident energy at which we evaluated the wave function or the incident electron, wave functions for the two outgoing electrons were evaluated at 31 pairs of selected k_1 and k_2 values satisfying Eq. (14). The 16 mesh points for $k_<$ contain ten equally spaced points and six points inserted at relatively small $k_<$ values. The corresponding mesh points for $k_>$ are decided by the mesh points for $k_<$ and Eq. (14). Here $k_<$ and $k_>$ represent the smaller and the larger of k_1 and k_2 , respectively. The continuum radial wave functions were computed up to a cutoff of 100 Bohr radii in a mesh of 1988 points. In evaluating Coulomb matrix elements, the contributions from the asymptotic region beyond the cutoff were computed.

The main contribution to the computer time in these calculations was from computation of Coulomb matrix elements. The maximum mesh used was 0.064 a.u., and Simpson's rule was used in evaluating integrals. For the cross section at 800 eV incident energy, the shortest wavelength of the continuum functions is 0.82, approximately 13 times the maximum mesh spacing. The calculations were not optimized with respect to computer time, and the total calculation required approximately 25 h on a CDC Cyber 855.

We calculated the diagrams of Figs. 1(d) and 1(e) using Eq. (15). We also calculated the diagrams of Figs. 2(a) through 2(e) and the other time ordering of Figs. 2(a) through 2(e). The summation over excited states k_3 in Figs. 2(a) through 2(d) were computed by the Dalgarno-Lewis method,^{29,30} and the potential in Eq. (18) was used for the k_3 orbitals.

For each incident partial wave kl , the allowed angular quantum numbers l_1 , l_2 , and l_3 for electrons k_1 , k_2 , and k_3 in the diagrams of Figs. 1 and 2 can be derived by considering the relation

$$v = \frac{1}{r_{ij}} = \sum_{\lambda=0}^{\infty} \frac{r_{<}^{\lambda}}{r_{>}^{\lambda+1}} P_{\lambda}(\hat{\mathbf{r}}_i \cdot \hat{\mathbf{r}}_j), \quad (19)$$

where P_{λ} denotes the λ th-order Legendre polynomial. The results for Fig. 1(d) are $|l-\lambda| \leq l_1 \leq |l+\lambda|$, $l_1 + l + \lambda = \text{even}$, and $l_2 = \lambda$. The allowed l_1 , l_2 , and l_3

TABLE I. The l values up to which 90% of the calculated σ is included.

Incident energy (eV)	l value ^a
50	5
100	8
200	14
400	24
800	44

^aThese results of low-order perturbation in general depend on the basis states used in the calculation.

values in other diagrams in Figs. 1 and 2 can be derived similarly.

Figure 1(d) was calculated including $\lambda=0 \rightarrow 4$ for the first 21 incident partial waves and including $\lambda=0 \rightarrow 2$ for some high- l partial waves at relatively high incident energies. At incident energy of 800 eV the highest partial wave we evaluated is the $l=50$ wave. We calculated Fig. 1(e) including $\lambda_1, \lambda_2=0 \rightarrow 4$ for all the incident partial waves for which this diagram is not zero. For incident energies below 10 eV, Figs. 1(d) and 1(e) were computed including $\lambda=0 \rightarrow 3$. The diagrams of Figs. 2(a) through 2(e) were calculated including $\lambda, \lambda_1, \lambda_2=0, 1$ for the first 21 partial waves.

For high incident energy values at which the partial cross section σ_2 for the highest evaluated partial wave is not very small, we approximately calculated σ_l for all the higher partial waves by extrapolating σ_l using a geometric series. The ratio taken between our calculated σ_{l+1} and σ_l shows an overall behavior of very slow increase with l at high l values and approaches an asymptotic value. For incident energy of 800 eV the asymptotic value is 0.955, and for lower energies the values are small. The geometric ratio we used in the extrapolation at each incident energy was an average of σ_{l+1} to σ_l ratios for the highest several partial waves that we evaluated.

In Table I for different incident energies we compare the l values of the partial waves up to which 90% of our result of σ are contributed. It shows how fast the contributions of high- l partial waves increase as the incident energy increases. In Table II we list contributions to σ

TABLE II. Cross section of He impact ionization calculated including different λ values. (These results of low-order perturbation calculations in general depend on the basis states used in the calculation.)

λ^a	σ (50 eV) (Mb)	σ (200 eV) (Mb)	σ (800 eV) (Mb)
0	6.607	3.855	1.037
1	30.408	30.726	12.842
2	30.666	34.949	14.853
3	30.190	35.424	15.227
4	30.040	35.262	15.338

^aThis λ value gives $\max\{\lambda\}$ in Fig. 1(a), $\max\{\lambda_1, \lambda_2\}$ in Fig. 1(b), and $\max\{\lambda\}$ in Figs. 2(a)–2(e). We only calculated the diagrams of Figs. 2(a)–2(e) including $\lambda, \lambda_1, \lambda_2=0, 1$. See Eq. (19) for the definition of λ .

obtained by increasing the values of λ , λ_1 , and λ_2 included in evaluating the diagrams. The results of Tables I and II also depend on the basis states used in this low-order perturbation calculation.

In Fig. 3 our results for σ are compared with results of recent experiments and other calculations. The results measured in recent years by Montague *et al.*,⁹ Wetzel *et al.*,¹⁰ and Krishnakumar and Srivastava¹¹ are very close to the results reported by Rapp and Englander-Golden in 1965.³¹ It can be seen that the agreement between the calculations and the experiments is good at high incident energies, and all calculated results are more or less too large near 100 eV.

The results calculated in the modified Born approximation by Bell and Kingston¹² and by Economides and McDowell¹⁴ are shown, and our results are about 10% lower than theirs at energies near 100 eV and quite close to theirs for energies higher than 400 eV. These authors have reviewed first Born calculations of the He electron-impact-ionization cross section.¹²⁻¹⁴ The length-modified Born cross section of Sloan¹⁵ and that of Bell and Kingston¹² differ by less than 1%. The length-modified Born results contributed by each partial wave of the ejected electron calculated by Peach¹⁶ agree well with the corresponding results of Bell and Kingston¹² except for the $l=0$ partial wave, and the discrepancy was attributed to the fact that in Peach's calculation the $1s$ and ks wave functions were not orthogonal. The results calculated by McGuire¹⁷ using wave functions based on the Herman-Skillman central potential are a little higher than those of Bell and Kingston¹² below 250 eV and are

in good agreement with them at higher energies.

The results of σ calculated by Bransden *et al.*³ using their distorted-wave model in three different approximations are plotted for comparison in Fig. 3. They used a second-order potential for orbitals of the incident electron and used polarization potentials and adiabatic approximations for orbitals of the outgoing electrons. The cross section of their $P1$ approximation, in which the orbitals of both the scattered (faster) and the ejected (slower) electrons were evaluated in the field of a He^+ ion, is about 10% higher than ours at incident energy of 100 eV and is the same as ours at about 400 eV. The cross section of their $P2$ approximation, in which the orbitals of the scattered electron were evaluated in the field of a neutral He atom, is about 20% higher than ours at 100 eV, but it decreases and remains a little lower than ours above 200 eV. They also computed σ using the results of $d\sigma/d\varepsilon$ interpolated from results of their $P1$ and $P2$ approximations, and in the interpolation $P1$ was used as the limit when the two outgoing electrons have the same energy, and $P2$ was the limit when the ejected electron has nearly zero energy. The resulting σ from the interpolated $d\sigma/d\varepsilon$ is lower than the results of both $P1$ and $P2$ approximations. This cross section is lower than ours by up to 7%. The results of Bartschat and Burke⁶ and Campeanu *et al.*¹⁷ are close to ours and are plotted in Fig. 4.

In Fig. 4 we compare our results of σ calculated in various approximations with results of experiments⁹⁻¹¹ and other calculations.^{6,7} The results are plotted against

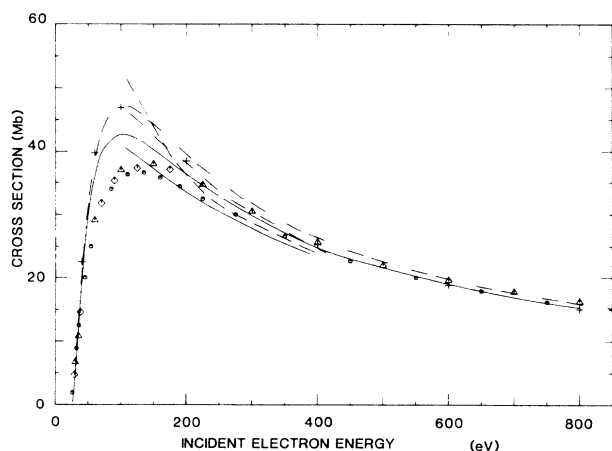


FIG. 3. Total ionization cross section σ of helium by electron impact. Circles, experimental results, Montague *et al.*, Ref. 9; triangles, experimental results, Krishnakumar and Srivastava, Ref. 11; diamonds, experimental results, Wetzel *et al.*, Ref. 10; +, the modified Born calculation of Economides and McDowell, Ref. 14. The geometric mean of their length and velocity form results is plotted. $-\cdots-$, the modified Born calculation of Bell and Kingston, Ref. 12; $-\cdot-\cdot-$, the distorted-wave approximation $P1$ of Bransden *et al.*, Ref. 3; $-\cdot-\cdot-$, the distorted-wave approximation $P2$ of Ref. 3; short solid curve, results from interpolated $d\sigma/d\varepsilon$, Ref. 3; longer solid curve, this work, the distorted-wave-exchange approximation (DWE) plus correlation effects in the initial state.

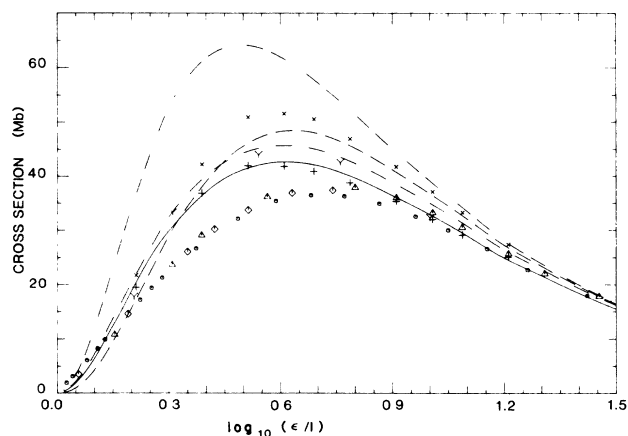


FIG. 4. Comparison of total cross sections in different approximations. The incident energy is denoted by ε_k , and I is the ionization energy. All the four curves were calculated in this work using orbitals based on potentials in Eqs. (17) and (18). $-\cdots-$, results of direct contributions given by Fig. 1(d); $-\cdot-\cdot-$, distorted-wave truncated approximation (DWT), Fig. 1(d) with $k_1 > k_2$; $-\cdot-\cdot-$, distorted-wave exchange approximation (DWE), Figs. 1(d) and 1(e); $-\cdot-\cdot-$, our final results, the DWE approximation plus correlation effects in the initial state, Figs. 1(d), 1(e), and 2(a)–2(e); \times , DWT results, Campeanu *et al.*, Ref. 7; +, DWE results, Campeanu, *et al.*, Ref. 7; Y , R -matrix calculation by Bartschat and Burke, Ref. 6; circles, diamonds, and triangles are experimental results from Refs. 9, 10, and 11, respectively.

the logarithm of the ratio between the incident energy and the ionization energy. All the calculated results are close to the measured results on the right-hand side of this figure but higher than the measured results in the intermediate range of this figure. Our results including only the direct contribution given by Fig. 1(d) can be seen as the highest curve in Fig. 4. One approximation method for including exchange contributions is to truncate the integration interval for the direct contribution at one-half, in analogy with the modified Born approximation. This approximation is referred to as the distorted-wave truncated (DWT) approximation,^{1,7} and the result corresponds to Fig. 1(d) with $k_1 > k_2$. Our DWT cross section is much smaller than the full direct contribution at low energies and gradually approaches it at high energies. Including both Figs. 1(d) and 1(e) corresponds to the distorted-wave exchange (DWE) approximation.^{1,7} Our DWE results are higher than our DWT results at lower energies but lower than the DWT results by up to 6% at higher energies, and this cross section also approaches the full direct contribution in the high energy limit. Our final results given by DWE plus correlation effects from Figs. 2(a) through 2(e) are lower than our DWE results in the whole energy range studied in this calculation. Our final results are lower than our DWE results by 4% at 800 eV incident energy, 7% at 100 eV incident energy, and 17% at 1 eV above the threshold. The correlation effects in the initial state decrease as the incident energy increases.

Campeanu *et al.*⁷ included polarization potentials in their distorted-wave approximations, and for the $1s$ orbital in the final-state wave function they used the orbital of the He^+ ion. They used a 158-point radial mesh extending to 18.7-bohr radii for the continuum states. Their DWT results are somewhat larger than our DWT results. Their DWE results are somewhat smaller than our DWE results but very close to our final results. Barschat and Burke⁶ used the R -matrix method to include electron correlation effects in their calculation, and they treated the exchange contribution by truncating the integration interval for the direct contribution. Their results are also close to our final results.

In Fig. 5 our final results of $d\sigma/d\varepsilon$ for incident energies of 50 eV, 300 eV, and 500 eV are plotted along with the experimental results of Opal *et al.*³² Results for $d\sigma/d\varepsilon$ are plotted versus the relative kinetic energies of the outgoing electrons with respect to the excess energy $\varepsilon_k - I$, where ε_k is the energy of the incident electron and I is the ionization energy. The Born results and Kingston at 50 and 500 eV are also plotted for comparison. We have symmetrized the results of Bell and Kingston with respect to the energies of the two outgoing electrons. It can be seen that the agreement between the calculated and the measured results is good for high incident energies and at 50 eV the calculated results are too high. Bell and Kingston¹³ had shown that at 2000 eV their Born results of $d\sigma/d\varepsilon$ were in excellent agreement with the experimental results of Opal *et al.*³² At 50 eV incident energy the Born results of Bell and Kingston are higher than our final results for all kinetic energies of the outgoing electrons, but at 500 eV the Born results of Bell and

Kingston are appreciably higher than our final results only when two outgoing electrons have similar kinetic energies.

In Fig. 6 our final results of $d\sigma/d\varepsilon$ at incident energies of 100 and 200 eV are compared with results of experiments and other calculations. All results at 100 eV have been multiplied by a factor of ten in plotting for clarity. The measured results are those of Opal *et al.*,³² Rudd and DuBois,³³ and Goodrich.³⁴ The agreement between the calculated and the measured results is better at the higher incident energy, and the Born results of Manson³⁵ are higher than ours. This is similar to the situation in Fig. 5. When the two outgoing electrons have similar kinetic energies, our results are somewhat higher than the $P1$ results of Bransden *et al.*³ and lower than their $P2$ results. At 100 eV incident energy and when an outgoing electron has very small energy, the $P2$ results of Bransden *et al.* are close to ours, and their $P1$ results are close to the Born results of Manson.³³ In Figs. 5 and 6, the curves of the $P2$ approximation of Bransden *et al.* and some curves of our results appear to have a cusp when the two outgoing electrons have the same energy. This is due to the fact that the continuum orbitals are

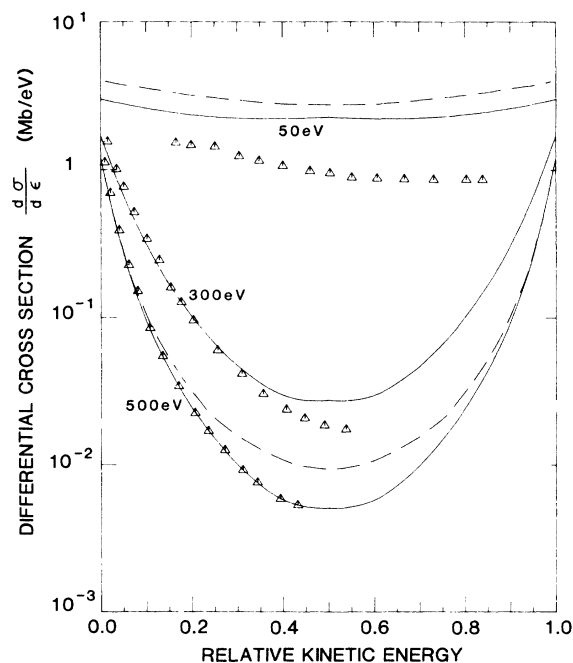


FIG. 5. Single-differential cross section $d\sigma/d\varepsilon$ of helium plotted vs relative kinetic energy $\varepsilon/(\varepsilon_k - I)$. The symbol ε is the kinetic energy of one outgoing electron, ε_k is the kinetic energy of the incident electron, and I is the ionization energy. Triangles, experimental results of Opal *et al.*, Ref. 32; —, present results, the distorted-wave approximation (DWE) plus correlation effects in the initial state; - - -, at incident energies of 50 and 500 eV, the Born calculation of Bell and Kingston, Ref. 13. We have symmetrized the results of Bell and Kingston with respect to the energies of the two outgoing electrons. The incident electron energy (50 eV, 300 eV, 500 eV) is shown in the figure.

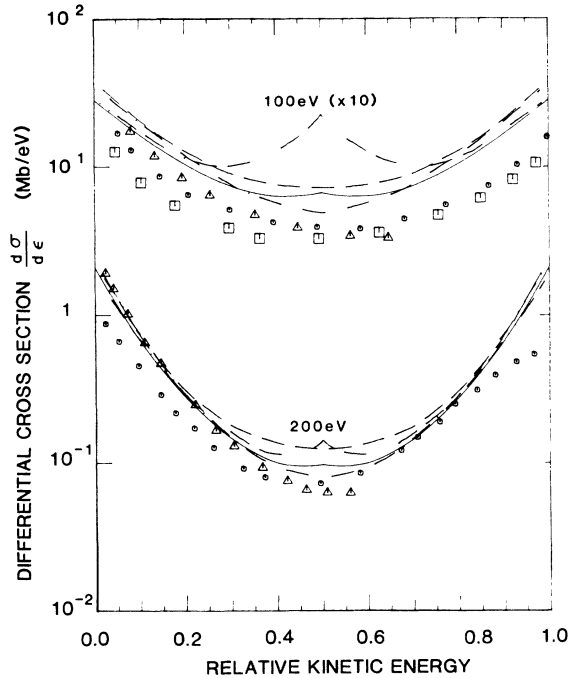


FIG. 6. Single-differential cross section $d\sigma/d\varepsilon$ of helium vs relative kinetic energy $\varepsilon/(\varepsilon_k - I)$. All results for incident energy 100 eV have been multiplied by a factor of 10 for clarity in presentation. Triangles, experimental results of Opal *et al.*, Ref. 32; circles, experimental results of Rudd and DeBois, Ref. 33; squares, experimental results of Goodrich, Ref. 34; —, present results, the distorted-wave approximation (DWE) plus correlation effects in the initial state; - - -, the Born calculation of Manson, Ref. 35; - · - · -, the distorted-wave approximation $P1$ of Bransden *et al.*, Ref. 3; - · - · -, the distorted-wave approximation $P2$ of Ref. 3.

evaluated in two different potentials according to their energies, which has been discussed by Bransden *et al.*³

For incident energies very close to the threshold, results of our various approximations using orbitals based on Eqs. (17) and (18) are all smaller than the experimental results. The threshold behavior of the electron-impact-ionization cross section has been studied by using the dynamical screening concept to approach the three-body problem involved in the impact-ionization processes.³⁶⁻⁴⁰ One of the conclusions is that in the stable solution for a double escape process, escaping electrons 1 and 2 leave the small reaction zone with a radius of a few bohr radii around the nucleus maintaining $r_1 = -r_2$, which is the condition for the Wannier saddle point.³⁶⁻⁴¹ According to this, we evaluated orbitals for both outgoing electrons using a simple potential which approximates the interaction experienced by each of the two electrons remaining on opposite sides of the nucleus at equal distances. The potential is

$$V_3 = V_1 + (1 - |1s\rangle\langle 1s|)[1.5J_{1s}^0 - (2/r) - V_1] \times (1 - |1s\rangle\langle 1s|), \quad (20)$$

where V_1 is given by Eq. (17). The asymptotic charge of potential V_3 is a half unit for all excited electrons.

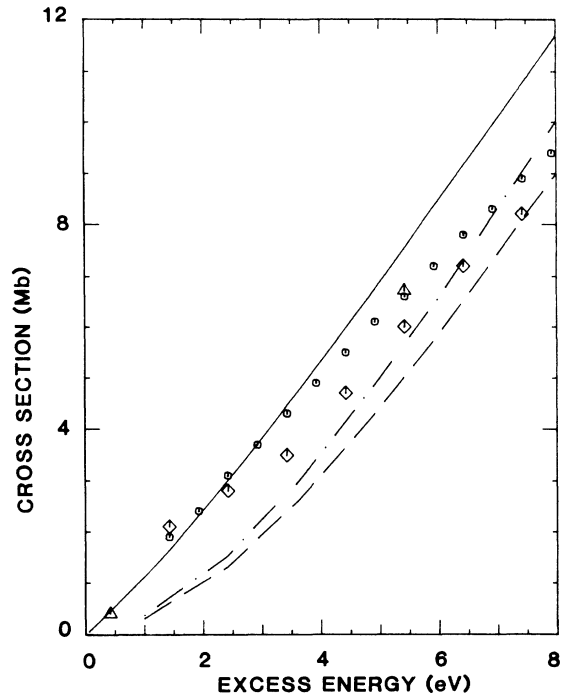


FIG. 7. Total cross section σ of helium near the ionization threshold vs excess energy $\varepsilon_k - I$, where ε_k is the energy of the incident electron. Circles, diamonds, and triangles are experimental results from Refs. 9, 10, and 11, respectively. —, results from outgoing waves based on Eq. (20), the distorted-wave exchange approximation (DWE); - - -, results from orbitals based on Eqs. (17) and (18), the DWE approximation plus correlation effects in the initial state; - · - · -, results based on Eqs. (17) and (18), the DWE approximation.

We calculated σ and $d\sigma/d\varepsilon$ for small excess energies using orbitals based on the potential of Eq. (20) for the two outgoing electrons. The diagrams of Figs. 1(d) and 1(e) were evaluated for $\lambda = 0 \rightarrow 3$, and the highest incident partial wave we included is the $l = 10$ wave. The results correspond to a distorted-wave exchange approximation with incident and outgoing waves based on the potentials of Eqs. (17) and (20), respectively.

In Fig. 7 we compare the results of σ with the experimental results for excess energies below 8 eV. Also shown are our results of σ using orbitals based on the potentials of Eqs. (17) and (18), which are too low near the threshold. The cross section using outgoing waves based on Eq. (20) agrees well with the measured results for excess energies below 4 eV but increases somewhat too fast as the energy increases above 4 eV. We did not include correlation effects in the initial state in the calculation using outgoing waves based on Eq. (20). When outgoing waves based on Eqs. (17) and (18), were used, the correlation effects in the initial state of the atom reduced the cross section at 1 eV excess energy by 17%.

In Fig. 8 we compare our results for $d\sigma/d\varepsilon$ in different distorted-wave approximations at excess energies of 1 and 6 eV. We also plotted the measured $d\sigma/d\varepsilon$ of Pichou *et al.*⁴² at excess energies of 1.4 and 6 eV. We show

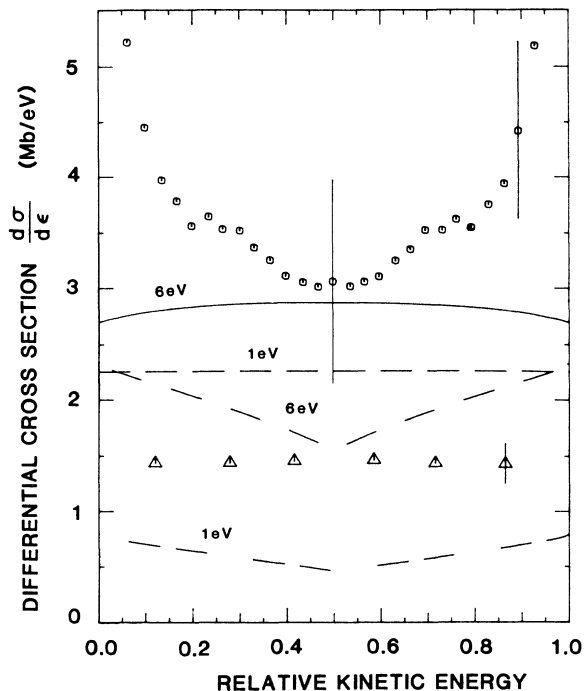


FIG. 8. Single-differential cross section $d\sigma/d\epsilon$ of helium near the ionization threshold. —, results from outgoing waves based on Eq. (20), the distorted-wave exchange approximation (DWE), at 6 eV excess energy; ---, DWE results based on Eq. (20), at 1 eV; - · - · -, results from orbitals based on Eqs. (17) and (18), the DWE approximation plus correlation effects in the initial state, at 6 eV; - · · · -, DWE plus initial state correlations, based on Eqs. (17) and (18), at 1 eV; Δ , results by Pichou *et al.*, Ref. 42, at 1.4 eV; \circ , results by Pichou *et al.*, at 6.0 eV, Ref. 42.

DWE results calculated using outgoing waves based on Eq. (20), and also the results of DWE plus initial-state correlation calculated using the orbitals based on Eqs. (17) and (18). It is clear that both the areas under the two curves of the same excess energy and the shapes of the two sets of curves are quite different. The energy distribution of the escaping electrons based on Eq. (20) is uniform at 1 eV excess energy, and it varies only by several percent as the energy increases to 6 eV. However, the energy distributions based on Eqs. (17) and (18) are nonuniform at both of the excess energies. This comparison suggests that the near-threshold results are very sensitive to potentials used for evaluating electron orbitals.

Experimental measurements for the energy distribution of the outgoing electrons for near-threshold electron-impact ionization of helium have been performed by Cvejanovic and Read,⁴³ Pichou *et al.*,⁴² Keenan *et al.*,⁴⁴ and Hammond *et al.*⁴⁵ Among these measurements only those of Pichou *et al.* are absolute results for $d\sigma/d\epsilon$,⁴² and all others are unnormalized. In 1974, Cvejanovic and Read⁴³ reported that the energy distribution was uniform within 15% for excess energies between 0.2 and 0.8 eV, and in 1985 Hammond *et al.*⁴⁵ reported essentially uniform distributions with 5% variation for excess energies from 0.075 to 0.6 eV. Pichou *et al.*⁴² measured

TABLE III. Partial cross sections of $kk'(^1L, ^3L)$ terms with $L \leq 4$. These results are based on the potential of Eq. (20) for orbitals of outgoing electrons.

Coupling terms ^{a, b}	σ (0.05 eV) ^c (10^{-3} Mb)	σ (0.10 eV) ^c (10^{-3} Mb)	σ (0.15 eV) ^c (10^{-3} Mb)
$^1S^e$	8.19	16.4	24.6
$^3S^e$	6.15×10^{-6}	7.69×10^{-5}	3.36×10^{-4}
$^1P^o$	6.69	13.4	20.2
$^3P^o$	8.90	17.8	26.8
$^1D^e$	25.0	50.3	75.8
$^3D^e$	0.441	0.907	1.40
$^1F^o$	1.68	3.48	5.39
$^3F^o$	0.831	1.72	2.68
$^{12}G^e$	0.0479	0.105	0.172
$^3G^e$	0.0150	0.0376	0.0669

^aIn the results for each $^1,^3L$ term, the contributions of different electron pairs kl and $k'l'$ were summed over as discussed in the text.

^bFor the electron-impact ionization of the ground state He atom, the L value and the parity of a $1skk'(^1,^3L)(^2L)$ final state are both even or both odd.

^cThe energy listed is excess energy $\epsilon_k - I$, where ϵ_k is the energy of the incident electron and I is the ionization energy.

$d\sigma/d\epsilon$ for excess energies up to 6 eV, and their results deviate from uniform behavior as the excess energy increases. They reported an accuracy of 40% for the absolute scale of their results. Their results are basically uniform at 1.4 eV excess energy, uniform within 20% at 3.6 eV, and nonuniform at 6 eV. However, Keenan *et al.*⁴⁴ later measured the energy distribution for excess energies up to 5.5 eV and reported that it was basically uniform up to 5.5 eV excess energy. Presently, the upper limit of excess energy for nearly uniform energy distribution of the outgoing electrons has not been completely determined.

TABLE IV. Partial cross sections of $klk'l'(^1,^3L)$ terms with $L \leq 3$. These results are based on the potential of Eq. (20) for orbitals of outgoing electrons. The three largest partial cross sections for each L value ($L \leq 3$) are listed here.

Coupling terms	σ (0.05 eV) ^a (10^{-3} Mb)
$ksk's(^1S)$	6.18
$kpk'p(^1S)$	2.01
$kdk'd(^1S)$	0.000 084 1
$ksk'p(^3P)$	8.88
$ksk'p(^1P)$	6.69
$kpk'd(^3P)$	0.0192
$kpk'p(^1D)$	25.0
$ksk'd(^3D)$	0.441
$ksk'd(^1D)$	0.005 83
$kpk'd(^1F)$	1.68
$kpk'd(^3F)$	0.828
$ksk'f(^3F)$	0.002 88

^aThese results were calculated for incident electrons with energies 0.05 eV in excess of the ionization energy.

In Table III we list the near-threshold partial cross section of each singlet or triplet coupling $^{1,3}L$ of the two outgoing electrons for $L=0 \rightarrow 4$. We calculated these results to compare with the existing theoretical studies on the threshold behavior of double-escape cross sections.³⁶⁻⁴⁰ Our results were calculated by using Eq. (13) and dropping the summation over the angular momentum couplings of the final states $\Phi_p^{k_1 k_2}$. Orbitals based on Eqs. (17) and (20) were used for the incident and outgoing waves, respectively. The partial cross sections of all these $^{1,3}L$ coupling terms increase approximately linearly as the excess energy increases, except that of $^3S^e$. The $^3S^e$ cross section varies with excess energy by a power greater than three. The very small cross section for the $^3S^e$ term is due to the strong cancellation between contributions from Figs. 1(d) and 1(e), and the results may be subject to some numerical error. When $L \neq 0$, two outgoing electrons with different angular quantum numbers can also contribute to each $^{1,3}L$ coupling term, and the 1L and 3L cross sections do not differ as much as the $L=0$ results differ due to cancellation. All the triplets contribute 19% of the total cross section at 0.05 eV excess energy. In Table IV we give more information about contributions from the largest ionization channels for $L=0 \rightarrow 3$ at excess energy 0.05 eV. The strongest ionization channel is $1skpk'p(^1D^e)(^2S)$, which contributes 48% of the total cross section at 0.05 eV excess energy.

According to theoretical studies³⁶⁻⁴⁰ on the threshold behavior of double-escape cross sections in the electron-impact ionization of a neutral atom, the partial cross sections for all the $^{1,3}L$ coupling terms vary with the excess energy by a power of 1.127, except those^{39,40} for $^3S^e$ and $^1P^e$, which vary by a power of 3.881. The $^3S^e$ and $^1P^e$ partial cross sections are suppressed at threshold since the wave functions are zero when the angle θ_{12} between the two outgoing electrons with respect to the nucleus is π for these cases.^{40,41} The energy distribution of the escaping electrons is uniform.^{36,37,40} In our low-order perturbation calculation the effects of the dynamical screening between the two outgoing electrons were not included, but our results based on the simple potential of Eq. (20) appear to agree reasonably with the above results. Another result of these studies^{40,41} is that the partial cross section of each $^{1,3}L$ coupling term, in which the L and S values and the parity are not all even or all odd, is reduced at the threshold because the wave function is zero when $\mathbf{r}_1 = -\mathbf{r}_2$. Our results do not violate this con-

clusion. In our results these types of coupling terms account for 17% of the total cross section at 0.05 eV excess energy, which is relatively small.

IV. CONCLUDING REMARKS

We calculated the total cross section σ and single-differential cross section $d\sigma/d\varepsilon$ for the electron-impact ionization of helium using the distorted-wave approximation and including correlation effects in the initial state of the atom. Electron correlations in the initial state were found to reduce the cross section by 17% at 1 eV excess energy and down to 4% at 800 eV incident kinetic energy. For incident energies below 150 eV the discrepancy between the results of experiments and calculations indicates the need for a more effective method to treat the interaction between the two outgoing electrons in the final state.

For low incident energies it is desirable to choose potentials which satisfy the relation of Eq. (16) better than the potentials derived from the assumption of complete screening of the residual ion by the slower outgoing electron. Improvement over the present agreement between calculated and measured total and single-differential cross sections appears possible by use of potentials with asymptotic charges depending on the kinetic energies of the outgoing electrons. Examples of such potentials have been discussed by Bransden *et al.*³

For incident energies near threshold, by using a simple potential which approximates the interaction experienced by each of the two electrons at $\mathbf{r}_1 = -\mathbf{r}_2$ we obtained results for σ which appear to agree reasonably with experimental results and results of studies based on Wannier theory and extensions thereof.³⁶⁻⁴⁰ For excess energies less than 6 eV, we found great variations in calculated results for $d\sigma/d\varepsilon$ according to which potential was used to calculate single particle states. In addition, the experimental situation for $d\sigma/d\varepsilon$ near 6 eV is somewhat unclear, and it would be desirable to have additional experimental information.

ACKNOWLEDGMENTS

This work was supported by the National Science Foundation. We are grateful to the Academic Computing Center of the University of Virginia for a computing grant.

¹S. M. Younger, Phys. Rev. A **22**, 111 (1980); **22**, 1425 (1980).

²H. Jakubowicz and D. L. Moores, J. Phys. B **14**, 3733 (1981); Comments At. Mol. Phys. **9**, 55 (1980).

³B. H. Bransden, J. J. Smith, and K. H. Winters, J. Phys. B **12**, 1267 (1979); **11**, 3095 (1978).

⁴M. S. Pindzola, D. C. Griffin, C. Bottcher, D. H. Crandall, R. A. Phaneuf, and D. C. Gregory, Phys. Rev. A **29**, 1749 (1984); P. G. Burke, W. C. Fon, and A. E. Kingston, J. Phys. B **17**, L733 (1984); R. I. Campeanu and L. Nagy, Z. Phys. A **321**, 371 (1985); S. M. Younger, Phys. Rev. A **35**, 2841 (1987); M. J. Roberts, J. Phys. B **21**, 1265 (1988).

⁵F. W. Byron, Jr., C. J. Joachain, and B. Piraux, J. Phys. B **19**, 1201 (1986); E. P. Curran and H. R. J. Walters, *ibid.* **20**, 337 (1987); F. M. Furtado and P. F. O'Mahony, *ibid.* **20**, L405 (1987); H. Klar, A. C. Roy, P. Schlemmer, K. Jung, and H. Ehrhardt, *ibid.* **20**, 821 (1987); R. J. Tweed and J. Langlois, *ibid.* **20**, 5213 (1987).

⁶K. Bartschat and P. G. Burke, J. Phys. B **20**, 3191 (1987).

⁷R. I. Campeanu, R. P. McEachran, and A. D. Stauffer, J. Phys. B **21**, 1411 (1988); **20**, 1635 (1987).

⁸A. F. Fetter and M. K. Watson, Adv. Theor. Phys. **1**, 115 (1965).

- ⁹R. G. Montague, M. F. A. Harrison, and A. C. H. Smith, *J. Phys. B* **17**, 3295 (1985).
- ¹⁰R. C. Wetzel, F. A. Baiocchi, T. R. Hayes, and R. S. Freund, *Phys. Rev. A* **35**, 559 (1987).
- ¹¹E. Krishnakumar and S. K. Srivastava, *J. Phys. B* **21**, 1055 (1988).
- ¹²K. L. Bell and A. E. Kingston, *J. Phys. B* **2**, 1125 (1969).
- ¹³K. L. Bell and A. E. Kingston, *Adv. At. Mol. Phys.* **10**, 53 (1974); *J. Phys. B* **3**, 1300 (1970).
- ¹⁴D. G. Economides and M. R. McDowell, *J. Phys. B* **2**, 1323 (1969).
- ¹⁵I. H. Sloan, *Proc. R. Soc. London, Ser. A* **281**, 151 (1964); *Proc. Phys. Soc. London* **85**, 435 (1965).
- ¹⁶G. Peach, *Proc. Phys. Soc. London* **85**, 709 (1965).
- ¹⁷E. J. McGuire, *Phys. Rev. A* **3**, 267 (1971).
- ¹⁸M. R. H. Rudge, *Rev. Mod. Phys.* **40**, 564 (1968).
- ¹⁹J. S. Bell and E. J. Squires, *Phys. Rev. Lett.* **3**, 96 (1959); M. Namiki, *Prog. Theor. Phys. (Kyoto)* **22**, 843 (1960).
- ²⁰D. J. Thouless, *The Quantum Mechanics of Many-Body Systems* (Academic, New York, 1961).
- ²¹R. T. Pu and E. S. Chang, *Phys. Rev.* **151**, 31 (1966); H. P. Kelly, *ibid.* **160**, 44 (1967); **171**, 54 (1968); M. Knowles and M. R. C. McDowell, *J. Phys. B* **6**, 300 (1973); B. S. Yarlagadda, G. Csanak, H. S. Taylor, B. Schneider, and R. Yaris, *Phys. Rev. A* **7**, 146 (1973); M. S. Pindzola and H. P. Kelly, *ibid.* **9**, 323 (1974); **11**, 221 (1975).
- ²²N. T. Padiyal, G. D. Meneses, F. J. da Paixao, Gy. Csanak, and D. C. Cartwright, *Phys. Rev. A* **23**, 2194 (1981); M. Ya. Amusia, N. A. Cherepkov, L. V. Chernysheva, D. M. Davidovic, and V. Radojevic, *ibid.* **25**, 219 (1982).
- ²³L. M. Frantz, R. L. Mills, R. G. Newton, and A. M. Sessler, *Phys. Rev. Lett.* **1**, 340 (1958); B. A. Lippmann, M. H. Mittleman, and K. M. Watson, *Phys. Rev.* **116**, 920 (1959); R. T. Pu and E. S. Chang, *ibid.* **151**, 31 (1966); H. J. Silverstone and M. L. Yin, *J. Chem. Phys.* **49**, 2026 (1968); S. Huzinaga and C. Arnau, *Phys. Rev. A* **1**, 1285 (1970).
- ²⁴H. A. Bethe, *Phys. Rev.* **57**, 1125 (1940).
- ²⁵S. L. Carter and H. P. Kelly, *Phys. Rev. A* **24**, 170 (1981).
- ²⁶R. K. Peterkop, *Zh. Eksp. Teor. Fiz.* **41**, 1938 (1961) [*Sov. Phys.—JETP* **14**, 1377 (1962)].
- ²⁷P. Nagy, A. Skutlartz, and V. Schmidt, *J. Phys. B* **13**, 1249 (1980).
- ²⁸H. E. Stanton and J. E. Monahan, *Phys. Rev.* **119**, 711 (1960).
- ²⁹A. Dalgarno and J. T. Lewis, *Proc. R. Soc. London, Ser. A* **233**, 70 (1955).
- ³⁰R. M. Sternheimer, *Phys. Rev.* **115**, 1198 (1959); **84**, 244 (1951).
- ³¹D. Rapp and P. Englander-Golden, *J. Chem. Phys.* **43**, 1464 (1965).
- ³²C. B. Opal, E. C. Beaty, and W. K. Peterson, *At. Data Nucl. Data Tables* **4**, 209 (1972).
- ³³M. E. Rudd and R. D. DuBois, *Phys. Rev. A* **16**, 26 (1977).
- ³⁴M. Goodrich, *Phys. Rev.* **52**, 259 (1937).
- ³⁵S. T. Manson, as presented in Ref. 33.
- ³⁶G. H. Wannier, *Phys. Rev.* **90**, 817 (1953).
- ³⁷A. R. P. Rau, *Phys. Rev. A* **4**, 207 (1971); *J. Phys. B* **9**, 1699 (1976).
- ³⁸R. Peterkop, *J. Phys. B* **4**, 513 (1971).
- ³⁹H. Klar and W. Schlecht, *J. Phys. B* **9**, 1699 (1976).
- ⁴⁰C. H. Greene and A. R. P. Rau, *Phys. Rev. Lett.* **48**, 533 (1982); *J. Phys. B* **16**, 99 (1983).
- ⁴¹A. D. Stauffer, *Phys. Lett.* **91A**, 114 (1982).
- ⁴²F. Pichou, A. Huetz, G. Joyez, and M. Landau, *J. Phys. B* **11**, 3683 (1978).
- ⁴³S. Cvejanovic and F. H. Read, *J. Phys. B* **7**, 1841 (1974).
- ⁴⁴G. A. Keenan, I. C. Walker, and D. F. Dance, *J. Phys. B* **15**, 2509 (1982).
- ⁴⁵P. Hammond, F. H. Read, S. Cvejanovic, and G. C. King, *J. Phys. B* **18**, L141 (1985).